EUROPEAN ORGANISATION FOR NUCLEAR RESEARCH

CERN-PPE/95-142
28 September 1995

Measurement of the $\tau^- \to e^- \bar{\nu}_e \nu_\tau$ Branching Ratio

The OPAL Collaboration

Abstract

The branching ratio of the $\tau^- \to e^- \bar{\nu}_e \nu_\tau$ decay mode has been measured with the OPAL detector to be $(17.78 \pm 0.10 \pm 0.09)\%$ where the first error is statistical and the second is systematic. The branching ratio, together with other measurements, has been used to test $e - \mu$ and $\mu - \tau$ universality in the charged current weak interaction.

(Submitted to Physics Letters B)

The OPAL Collaboration

G. Alexander[23], J. Allison[16], N. Altekamp[5], K. Ametewee[25], K.J. Anderson[9], S. Anderson[12], S. Arcelli[2], S. Asai[24], D. Axen[29], G. Azuelos[18,a], A.H. Ball[17], E. Barberio[26], R.J. Barlow[16], R. Bartoldus[3], J.R. Batley[5], G. Beaudoin[18], J. Bechtluft[14], G.A. Beck[13], C. Beeston[16], T. Behnke[8], A.N. Bell[1], K.W. Bell[20], G. Bella[23], S. Bentvelsen[8], P. Berlich[10], S. Bethke[14], O. Biebel[14], I.J. Bloodworth[1], J.E. Bloomer[1], P. Bock[11], H.M. Bosch[11], M. Boutemeur[18], B.T. Bouwens[12], S. Braibant[12], P. Bright-Thomas[25], R.M. Brown[20], H.J. Burckhart[8], C. Burgard[27], R. Bürgin[10], P. Capiluppi[2], R.K. Carnegie[6], A.A. Carter[13], J.R. Carter[5], C.Y. Chang[17], C. Charlesworth[6], D.G. Charlton[1,b], D. Chrisman[4], S.L. Chu[4], P.E.L. Clarke[15], S.G. Clowes[16], I. Cohen[23], J.E. Conboy[15], O.C. Cooke[16], M. Cuffiani[2], S. Dado[22], C. Dallapiccola[17], G.M. Dallavalle[2], C. Darling[31], S. De Jong[12], L.A. del Pozo[8], M.S. Dixit[7], E. do Couto e Silva[12], E. Duchovni[26], G. Duckeck[8], I.P. Duerdoth[16], U.C. Dunwoody[8], J.E.G. Edwards[16], P.G. Estabrooks[6], H.G. Evans[9], F. Fabbri[2], B. Fabbro[21], P. Fath[11], F. Fiedler[12], M. Fierro[2], M. Fincke-Keeler[28], H.M. Fischer[3], R. Folman[26], D.G. Fong[17], M. Foucher[17], H. Fukui[24], A. Fürtjes[8], P. Gagnon[7], A. Gaidot[21], J.W. Gary[4], J. Gascon[18], S.M. Gascon-Shotkin[17], N.I. Geddes[20], C. Geich-Gimbel[3], S.W. Gensler[9], F.X. Gentit[21], T. Geralis[20], G. Giacomelli[2], P. Giacomelli[4], R. Giacomelli[2], V. Gibson[5], W.R. Gibson[13], D.M. Gingrich[30,a], J. Goldberg[22], M.J. Goodrick[5], W. Gorn[4], C. Grandi[2], E. Gross[26], C. Hajdu[32], G.G. Hanson[12], M. Hansroul[8], M. Hapke[13], C.K. Hargrove[7], P.A. Hart[9], C. Hartmann[3], M. Hauschild[8], C.M. Hawkes[8], R. Hawkings[8], R.J. Hemingway[6], G. Herten[10], R.D. Heuer[8], M.D. Hildreth[8], J.C. Hill[5], S.J. Hillier[8], T. Hilse[10], P.R. Hobson[25], D. Hochman[26], R.J. Homer[1], A.K. Honma[28,a], D. Horváth[32,c], R. Howard[29], R.E. Hughes-Jones[16], D.E. Hutchcroft[5], P. Igo-Kemenes[11], D.C. Imrie[25], A. Jawahery[17], P.W. Jeffreys[20], H. Jeremie[18], M. Jimack[1], A. Joly[18], M. Jones[6], R.W.L. Jones[8], U. Jost[11], P. Jovanovic[1], D. Karlen[6], T. Kawamoto[24], R.K. Keeler[28], R.G. Kellogg[17], B.W. Kennedy[20], B.J. King[8], J. King[13], J. Kirk[29], S. Kluth[5], T. Kobayashi[24], M. Kobel[10], D.S. Koetke[6], T.P. Kokott[3], S. Komamiya[24], R. Kowalewski[8], T. Kress[11], P. Krieger[6], J. von Krogh[11], P. Kyberd[13], G.D. Lafferty[16], H. Lafoux[21], R. Lahmann[17], W.P. Lai[19], D. Lanske[14], J. Lauber[15], J.G. Layter[4], A.M. Lee[31], E. Lefebvre[18], D. Lellouch[26], J. Letts[2], L. Levinson[26], C. Lewis[15], S.L. Lloyd[13], F.K. Loebinger[16], G.D. Long[17], B. Lorazo[18], M.J. Losty[7], J. Ludwig[10], A. Luig[10], A. Malik[21], M. Mannelli[8], S. Marcellini[2], C. Markus[3], A.J. Martin[13], J.P. Martin[18], G. Martinez[17], T. Mashimo[24], W. Matthews[25], P. Mättig[3], W.J. McDonald[30], J. McKenna[29], E.A. Mckigney[15], T.J. McMahon[1], A.I. McNab[13], F. Meijers[8], S. Menke[3], F.S. Merritt[9], H. Mes[7], J. Meyer[27], A. Michelini[8], G. Mikenberg[26], D.J. Miller[15], R. Mir[26], W. Mohr[10], A. Montanari[2], T. Mori[24], M. Morii[24], U. Müller[3], B. Nellen[3], B. Nijjhar[16], R. Nisius[8], S.W. O'Neale[1], F.G. Oakham[7], F. Odorici[2], H.O. Ogren[12], N.J. Oldershaw[16], T. Omori[24], C.J. Oram[28,a], M.J. Oreglia[9], S. Orito[24], M. Palazzo[2], J. Pálinkás[33], J.P. Pansart[21], G. Pásztor[33], J.R. Pater[16], G.N. Patrick[20], M.J. Pearce[1], P.D. Phillips[16], J.E. Pilcher[9], J. Pinfold[30], D.E. Plane[8], P. Poffenberger[28], B. Poli[2], A. Posthaus[3], T.W. Pritchard[13], H. Przysiezniak[30], D.L. Rees[1], D. Rigby[1], M.G. Rison[5], S.A. Robins[13], N. Rodning[30], J.M. Roney[28], E. Ros[8], A.M. Rossi[2], M. Rosvick[28], P. Routenburg[30], Y. Rozen[8], K. Runge[10], O. Runolfsson[8], D.R. Rust[12], R. Rylko[25], E.K.G. Sarkisyan[23], M. Sasaki[24], C. Sbarra[2], A.D. Schaile[8], O. Schaile[10], F. Scharf[3], P. Scharff-Hansen[8], P. Schenk[4], B. Schmitt[3], M. Schröder[8], H.C. Schultz-Coulon[10], M. Schulz[8], P. Schütz[3], J. Schwiening[3], W.G. Scott[20], T.G. Shears[16], B.C. Shen[4], C.H. Shepherd-Themistocleous[27], P. Sherwood[15], G.P. Siroli[2], A. Sittler[27], A. Skillman[15], A. Skuja[17], A.M. Smith[8], T.J. Smith[28], G.A. Snow[17], R. Sobie[28], S. Söldner-Rembold[10],

R.W. Springer[30], M. Sproston[20], A. Stahl[3], M. Starks[12], C. Stegmann[10], K. Stephens[16], J. Steuerer[28], B. Stockhausen[3], D. Strom[19], F. Strumia[8], P. Szymanski[20], R. Tafirout[18], H. Takeda[24], P. Taras[18], S. Tarem[26], M. Tecchio[8], N. Tesch[3], M.A. Thomson[8], E. von Törne[3], S. Towers[6], M. Tscheulin[10], T. Tsukamoto[24], E. Tsur[23], A.S. Turcot[9], M.F. Turner-Watson[8], P. Utzat[11], R. Van Kooten[12], G. Vasseur[21], P. Vikas[18], M. Vincter[28], E.H. Vokurka[16], F. Wäckerle[10], A. Wagner[27], D.L. Wagner[9], C.P. Ward[5], D.R. Ward[5], J.J. Ward[15], P.M. Watkins[1], A.T. Watson[1], N.K. Watson[7], P. Weber[6], P.S. Wells[8], N. Wermes[3], B. Wilkens[10], G.W. Wilson[27], J.A. Wilson[1], T. Wlodek[26], G. Wolf[26], S. Wotton[11], T.R. Wyatt[16], S. Xella[2], S. Yamashita[24], G. Yekutieli[26], V. Zacek[18],

[1]School of Physics and Space Research, University of Birmingham, Birmingham B15 2TT, UK
[2]Dipartimento di Fisica dell' Università di Bologna and INFN, I-40126 Bologna, Italy
[3]Physikalisches Institut, Universität Bonn, D-53115 Bonn, Germany
[4]Department of Physics, University of California, Riverside CA 92521, USA
[5]Cavendish Laboratory, Cambridge CB3 0HE, UK
[6] Ottawa-Carleton Institute for Physics, Department of Physics, Carleton University, Ottawa, Ontario K1S 5B6, Canada
[7]Centre for Research in Particle Physics, Carleton University, Ottawa, Ontario K1S 5B6, Canada
[8]CERN, European Organisation for Particle Physics, CH-1211 Geneva 23, Switzerland
[9]Enrico Fermi Institute and Department of Physics, University of Chicago, Chicago IL 60637, USA
[10]Fakultät für Physik, Albert Ludwigs Universität, D-79104 Freiburg, Germany
[11]Physikalisches Institut, Universität Heidelberg, D-69120 Heidelberg, Germany
[12]Indiana University, Department of Physics, Swain Hall West 117, Bloomington IN 47405, USA
[13]Queen Mary and Westfield College, University of London, London E1 4NS, UK
[14]Technische Hochschule Aachen, III Physikalisches Institut, Sommerfeldstrasse 26-28, D-52056 Aachen, Germany
[15]University College London, London WC1E 6BT, UK
[16]Department of Physics, Schuster Laboratory, The University, Manchester M13 9PL, UK
[17]Department of Physics, University of Maryland, College Park, MD 20742, USA
[18]Laboratoire de Physique Nucléaire, Université de Montréal, Montréal, Quebec H3C 3J7, Canada
[19]University of Oregon, Department of Physics, Eugene OR 97403, USA
[20]Rutherford Appleton Laboratory, Chilton, Didcot, Oxfordshire OX11 0QX, UK
[21]CEA, DAPNIA/SPP, CE-Saclay, F-91191 Gif-sur-Yvette, France
[22]Department of Physics, Technion-Israel Institute of Technology, Haifa 32000, Israel
[23]Department of Physics and Astronomy, Tel Aviv University, Tel Aviv 69978, Israel
[24]International Centre for Elementary Particle Physics and Department of Physics, University of Tokyo, Tokyo 113, and Kobe University, Kobe 657, Japan
[25]Brunel University, Uxbridge, Middlesex UB8 3PH, UK
[26]Particle Physics Department, Weizmann Institute of Science, Rehovot 76100, Israel
[27]Universität Hamburg/DESY, II Institut für Experimental Physik, Notkestrasse 85, D-22607 Hamburg, Germany
[28]University of Victoria, Department of Physics, P O Box 3055, Victoria BC V8W 3P6, Canada

[29]University of British Columbia, Department of Physics, Vancouver BC V6T 1Z1, Canada
[30]University of Alberta, Department of Physics, Edmonton AB T6G 2J1, Canada
[31]Duke University, Dept of Physics, Durham, NC 27708-0305, USA
[32]Research Institute for Particle and Nuclear Physics, H-1525 Budapest, P O Box 49, Hungary
[33]Institute of Nuclear Research, H-4001 Debrecen, P O Box 51, Hungary

[a]Also at TRIUMF, Vancouver, Canada V6T 2A3
[b] Royal Society University Research Fellow
[c] Institute of Nuclear Research, Debrecen, Hungary

The $\tau^- \to e^- \bar{\nu}_e \nu_\tau$ decay is a useful probe of the Standard Model. The branching ratio, in conjunction with other measurements, can be used to determine the relative charged current couplings of the electron, muon and tau leptons. In addition, it can be used to calculate α_s at $Q^2 = M_\tau^2$, which can be compared with other measurements taken at $Q^2 = M_Z^2$. This letter reports on an update of the $\tau^- \to e^- \bar{\nu}_e \nu_\tau$ branching ratio using the data collected between 1991 and 1994 with the OPAL detector at LEP.

The data were recorded using the OPAL detector which is a general purpose detector covering the full solid angle [1]. The tau pair Monte Carlo sample was generated using the KORALZ 4.0 package [2]. The dynamics of the tau decays were simulated with the TAUOLA 2.0 decay library [3]. The Monte Carlo events were then passed through the GEANT simulation [4] of the OPAL detector [5].

The procedure used to select $Z^0 \to \tau^+\tau^-$ events is similar to that described in previous OPAL publications [6, 7, 8]. The decay of the Z^0 produces two back-to-back taus. The taus are highly relativistic so that the decay products are strongly collimated. As a result it is convenient to treat each τ decay as a jet, as defined in ref.[9], where charged tracks and clusters in the lead-glass electromagnetic calorimeter are assigned to cones of half-angle 35°. The definitions of a charged track and electromagnetic cluster are also given in references [6, 7, 8]. The tau pair selection requires that the event contains exactly two jets each with at least one charged track. The total electromagnetic energy plus the sum of the scalar momentum of the charged tracks in each jet must exceed 1% of the beam energy. The average value of $|\cos\theta|$ for the two charged jets must satisfy $\overline{|\cos\theta|} < 0.68$, where θ is the polar angle, to avoid regions of non-uniform response in the lead-glass calorimeter.

The background in the $\tau^+\tau^-$ sample includes contributions from the $e^+e^- \to e^+e^-$ [10], $e^+e^- \to \mu^+\mu^-$ [2], $e^+e^- \to q\overline{q}$ [11] and $e^+e^- \to (e^+e^-)X$ [12] reactions. The background from $e^+e^- \to e^+e^-$ events can be identified by the presence of two high-momentum, back-to-back charged particles with the full centre-of-mass energy ($E_{\rm CM}$) deposited in the lead-glass electromagnetic calorimeter. This background is reduced by requiring the tau pair candidates to satisfy either $E_{\rm cluster} \leq 0.8 E_{\rm CM}$ or $E_{\rm cluster} + 0.3 E_{\rm track} \leq E_{\rm CM}$, where $E_{\rm cluster}$ is the total energy in the lead-glass calorimeter and $E_{\rm track}$ is the sum of the scalar momentum of the charged tracks in the event. Note that the $e^+e^- \to e^+e^-$ rejection requirements are slightly different from those used in ref. [8]. The first criterion eliminates most of the $e^+e^- \to e^+e^-$ background while the second criterion eliminates $e^+e^- \to e^+e^-$ events that have two high momentum tracks but do not deposit all of their energy in the electromagnetic calorimeter (for example, there are regions of poor energy resolution in the calorimeter due to the support structure).

Events from the $e^+e^- \to \mu^+\mu^-$ reaction can also be identified by the presence of two high-momentum, back-to-back charged particles with very little energy deposited in the lead-glass electromagnetic calorimeter. These events are rejected if they pass the muon pair selection described in ref. [6, 7, 8]. Multihadronic decays of the Z^0 ($e^+e^- \to q\overline{q}$) are removed by requiring that each event contain 2-6 charged tracks and less than 10 clusters in the lead-glass electromagnetic calorimeter. The background from $e^+e^- \to (e^+e^-)X$ (two-photon) events, where the final-state electron and positron escape undetected at low angles, is suppressed by requiring the acolinearity between the two jets to be less than 15°. The visible energy, $E_{\rm visible} = E_{\rm cluster} + E_{\rm track}$, of the two-photon system is in general much smaller than that from a tau pair event, hence an event is rejected if $E_{\rm visible} \leq 0.03 E_{\rm CM}$. Furthermore, if $E_{\rm visible} \leq 0.2 E_{\rm CM}$, then the event

is rejected if the missing transverse momenta, calculated separately for charged tracks and for lead-glass clusters, are both less than 2 GeV/c.

The fraction of background in the tau pair sample is found to be 0.0170 ± 0.0012. The contributions from the individual channels are given in Table 1. The $e^+e^- \to q\overline{q}$ and $e^+e^- \to (e^+e^-)\,\mu^+\mu^-$ background estimates have not changed from ref. [8]. The $e^+e^- \to \mu^+\mu^-$, $e^+e^- \to e^+e^-$ and $e^+e^- \to (e^+e^-)\,e^+e^-$ backgrounds have been re-evaluated since they are a significant background in either the tau pair sample or the $\tau^- \to e^-\bar{\nu}_e\nu_\tau$ sample. The backgrounds have been estimated by Monte Carlo and confirmed by comparisons with data in a manner similar to that presented in ref. [8]. Other potential backgrounds arising from cosmic rays and single-beam interactions are suppressed with simple requirements on the time-of-flight detector and on the location of the primary event vertex. These selection criteria were applied to all the data collected from 1991 to 1994 to give a sample of 82 808 $\tau^+\tau^-$ candidate events.

The selection of electron candidates is divided into two parts: a 'Fiducial' selection followed by an 'Electron Identification' selection. The Fiducial selection applies criteria that are independent of the particle type (such as fiducial cuts). The efficiency for this selection is determined entirely from data samples. The Electron Identification selection applies criteria that separate electrons from muons and hadrons. For this selection the efficiency is estimated using Monte Carlo samples and systematic studies comparing data and Monte Carlo samples are done to estimate the uncertainty.

The Fiducial selection requires that the candidate jet have between 1 and 3 charged tracks. Regions of the detector where the z-measuring tracking chamber or 'z-chamber' [1] was not active and the regions of poor energy resolution in the electromagnetic calorimeter are eliminated. Also, we apply additional requirements on the tracks. The highest momentum track in each jet, assumed to be the electron candidate, must have hits in the z-chambers in order to improve the polar angular resolution. In addition, we require that each track have at least 40 hits in the central drift chamber that can be used in the measurement of the energy loss (dE/dx).

The efficiencies for the Fiducial selection were determined using the entire tau data sample and are given in Table 2. Note that the efficiencies for the z-chamber and $\mathrm{d}E/\mathrm{d}x$-hits used in the branching ratio calculation were determined as a function of momentum but only average values are given in Table 2. The z-chamber and $\mathrm{d}E/\mathrm{d}x$ hit efficiencies for jets with 1 charged track were tested to see if they were independent of the particle type using control samples of electron data. The systematic errors quoted on these efficiencies (see Table 2) represents the precision with which this assumption was tested.

The Electron Identification selection identifies the electron candidates out of the tau sample remaining after the Fiducial selection. The Electron Identification selection relies on a relatively small set of variables in order to achieve high efficiency with low background. A number of the variables have been transformed into normalized quantities, $N_V^\sigma \equiv (V_{measured} - V_{expected})/\sigma_V$, where $V_{measured}$ is the variable of interest, $V_{expected}$ is the expected mean value and σ_V is its rms.

The selection requires that the primary or highest momentum track in the jet has a $\mathrm{d}E/\mathrm{d}x$

[1] A right-handed coordinate system is adopted in OPAL, where the x axis points to the centre of the LEP ring, and positive z is along the electron beam direction. The angles θ and ϕ are the polar and azimuthal angles, respectively.

measurement ($N^{\sigma}_{dE/dx} \geq -3$) compatible with that expected from an electron (see fig. 1(a)). An electromagnetic cluster (θ_{cl}, ϕ_{cl}) is considered associated to a charged track (θ_{tk}, ϕ_{tk}) if $|\Delta\theta \equiv \theta_{cl} - \theta_{tk}| \leq 0.040$ radians and $|\Delta\phi \equiv \phi_{cl} - \phi_{tk}| \leq 0.040$ radians. (Note that (θ_{tk}, ϕ_{tk}) is the extrapolated track position at the front face of the electromagnetic calorimeter.) If there is a cluster (with energy E) associated to the track (with momentum p), then the ratio E/p ($N^{\sigma}_{E/p} \geq -4$) is used to remove muons and pions (see fig. 1(b)). If there is no cluster associated to the track, then this criterion is not applied.

Even though the lead-glass blocks of the calorimeter are typically 0.040 radians wide in both θ and ϕ, the cluster position for electromagnetic showers is known to better than 0.003 radians if the energy is shared between at least two lead-glass blocks. We use this information by placing requirements on the $N^{\sigma}_{\Delta\theta}$ and $N^{\sigma}_{\Delta\phi}$ distributions (see Fig. 1(c) and (d)). The value for σ used in these normalized quantities ranges between 1 and 7 milliradians depending on the track momentum and energy distribution in the cluster. Matching in θ is found to be a good filter against background from pions. The matching in ϕ is complicated by the magnetic field and by photon radiation. In addition, the modelling of $N^{\sigma}_{\Delta\phi}$ is not particularly good for large positive values. As a result a looser matching criterion is applied in ϕ than in θ.

Photons that appear in $\tau^- \rightarrow e^- \bar{\nu_e} \nu_\tau$ jets originate from either final state radiation or bremsstrahlung radiation. Photons from initial state radiation are emitted in a direction close to the beam axis and are therefore not included in the jets while photons from final state radiation are isotropically distributed about the jet axis. Bremsstrahlung photons are emitted in a narrow cone. If the charge of the track is positive/negative, the field bends the track from its initial ϕ_i value toward a higher/lower final ϕ_f value. Photons from this track are then observed in a 0.020 radians wide band in θ in the electromagnetic calorimeter with ϕ values between ϕ_f and ϕ_i.

A cluster (θ_{cl}, ϕ_{cl}) is considered a photon candidate if its energy is greater than 0.7 GeV and there is no charged track (θ_{tk}, ϕ_{tk}) nearby ($|\theta_{cl} - \theta_{tk}| \geq 0.040$ radians or $|\phi_{cl} - \phi_{tk}| \geq 0.040$ radians). The electron selection allows up to one such cluster in a jet (see fig. 1(e)). In addition, clusters found in a 0.020 radian band in θ and with ϕ values between the initial and final values of the track are not counted, as discussed in the previous paragraph.

The hadron calorimeter is also used in the electron selection. It consists of 8 iron slabs of 0.6 interaction lengths thickness interleaved with 9 detection layers. There are approximately 2.2 interaction lengths of material in front of the hadron calorimeter. We require that the electron candidate penetrate no further than 2 layers (0.6 interaction lengths) into the hadron calorimeter (see fig. 1(f)).

As indicated earlier, a small background of $e^+e^- \rightarrow e^+e^-$ events remain in the tau pair sample. The Electron Identification selection we have described so far would not reject these events and consequently we add an extra criterion that removes most of them from the $\tau^- \rightarrow e^- \bar{\nu_e} \nu_\tau$ sample. We observed that a significant number of the $e^+e^- \rightarrow e^+e^-$ events in the tau pair sample consist of two back-to-back, high momentum tracks. Thus we can reduce the $e^+e^- \rightarrow e^+e^-$ background by requiring that $\theta_{acop} > 0.002$ radians if both $p > 30$ GeV/c and $p_{opp} > 0.75 E_{beam}$, where θ_{acop} is the acoplanarity angle in the plane transverse to the beam between the highest momentum tracks in each jet, p is the momentum of the electron candidate, p_{opp} is the momentum of the track in the jet opposite the electron candidate and E_{beam} is the

beam energy.

The Electron Identification selection also accepts jets with 2 or 3 charged tracks. The highest momentum track is taken to be the electron and the remaining tracks are considered to be the result of a photon conversion. For jets with 2 charged tracks we assume that one track from the photon conversion went undetected. The second track is required to have a $\mathrm{d}E/\mathrm{d}x$ measurement that is consistent with being an electron and a momentum of less than 3 GeV/c. For jets with 3 charged tracks, we require that both tracks have a $\mathrm{d}E/\mathrm{d}x$ measurement that is consistent with being an electron, a combined scalar momentum of less than 5 GeV/c and a mass (calculated from the two tracks) of less than 0.1 GeV/c^2. The efficiency for selecting electrons in these jets is approximately 80% compared with approximately 99% for jets with only a single track due to the additional selection criteria. Approximately 1.5% of the electron candidates are composed of 2 and 3 charged track jets.

A total of 25 337 candidates pass the electron selection with an Electron Identification efficiency, ϵ_E, of 0.9893 ± 0.0027 and a background, f_{bkgd}^{non-e}, of 0.0496 ± 0.0031. These results give a branching ratio of the $\tau^- \rightarrow \mathrm{e}^-\bar{\nu}_\mathrm{e}\nu_\tau$ decay of $(17.78 \pm 0.10(stat) \pm 0.09(syst))\%$. The branching ratio was calculated using

$$B_e = \frac{N_e^{corr}}{N_\tau\,(1 - f_{bkgd}^{non-\tau})} \frac{1 - f_{bkgd}^{non-e}}{\epsilon_E} \frac{1}{F_{bias}^e}$$

where N_τ is the number of taus (165 616), $f_{bkgd}^{non-\tau}$is the background in the tau sample (0.0170 ± 0.0012) and F_{bias}^e is a correction for the slight bias on the branching ratio introduced by the tau pair selection (1.0036 ± 0.0022). The number of electrons, N_e^{corr}, in the above equation is corrected for the Fiducial selection efficiencies (given in Table 2) by

$$N_e^{corr} = \sum_{i=1}^{10} \frac{N_e^{1tk}(i)}{\epsilon_F^{1tk}(i)} + \frac{N_e^{2tk}}{\epsilon_F^{2tk}} + \frac{N_e^{3tk}}{\epsilon_F^{3tk}}$$

where N_e is the number of electron candidates and ϵ_F is the Fiducial selection efficiency. The superscripts indicate the number of charged tracks in the jet. The summation is performed over 10 momentum bins for jets with 1 charged track. The average Fiducial selection efficiency for jets with 1 charged track is 0.8395 ± 0.0020 where the error is dominated by the systematic error in the z-chamber hit efficiency. Using the average efficiencies will give a branching ratio similar to the quoted value.

The contributions to the systematic error are given in Table 3. The uncertainty in the efficiency of the electron selection and the uncertainty in the background in the electron sample are discussed in the following paragraphs. The photon conversion systematic error arises as the Monte Carlo has a slightly different probability for a photon conversion from that observed in the data. However since jets with up to three charged tracks are permitted into the sample, the dependence of the final result on this probability was found to be fairly weak.

The Electron Identification efficiency was determined using Monte Carlo. The efficiency was found to be independent of momentum over the entire range ($0 \leq x \equiv p/E_{beam} \leq 1$). The largest deviation in any of the 20 equally sized x-bins was seen to be 0.5%, while most are well below the 0.25% level. To test the validity of the Monte Carlo, the efficiency of each criterion in the selection was determined using highly pure control samples of electrons obtained

by applying tight cuts to the tau sample. Comparisons of the efficiencies obtained from the Monte Carlo and data control samples showed no inconsistencies. For example, we found the efficiency of the dE/dx criterion to be 0.99562 ± 0.00126 and 0.99662 ± 0.00102 in the data and Monte Carlo, respectively. Since the efficiencies from the data and Monte Carlo were in good agreement, we assign a systematic error to the Electron Identification efficiency of 0.0016 for the dE/dx requirement which is obtained by adding in quadrature the statistical errors of the data and Monte Carlo efficiencies.

This procedure was repeated for each criterion in the Electron Identification selection. We found no disagreement between the efficiencies found with the data and Monte Carlo samples. A systematic error for each criterion was determined by adding in quadrature the statistical errors of the data and Monte Carlo efficiencies. The total systematic error on the efficiency, 0.0026, is the quadratic sum of the errors from each selection criteria. The largest contribution is from the dE/dx criterion as it has the lowest efficiency. We combine the systematic error, 0.0026, with the statistical uncertainty of 0.0008, to obtain a total error of 0.0027 on the Electron Identification efficiency. Consequently the error on the branching ratio due to the uncertainty on the Electron Identification selection efficiency is estimated to be 0.00048 (see Table 3).

Additional checks of the uncertainty on the Electron Identification efficiency were made. These studies used samples of $e^+e^- \to e^+e^-$ and $e^+e^- \to (e^+e^-)e^+e^-$ data. No discrepancy between the efficiencies found from each of the cross checks and those obtained from the tau samples were found. As a result no additional uncertainty was added to the efficiency.

The reliability of the branching ratio was investigated further by varying the individual selection requirements. The range of the variations were chosen so that the background in the new sample did not significantly change to avoid generating a large systematic uncertainty. In addition, we removed the requirement that the tracks have hits in the z-chamber. Removing the z-chamber requirement degrades the θ resolution of the tracks, consequently in this check we also dropped our θ track-cluster matching requirement. This increased the data sample by approximately 10% but also increased the background. However, the branching ratio obtained with this sample was found to be in good agreement with our result as well as with the branching ratio obtained from a separate electron selection.

The background in the $\tau^- \to e^- \bar{\nu}_e \nu_\tau$ sample is broken down into its various sources in Table 1. The backgrounds were first estimated using Monte Carlo samples. The modelling of each of the backgrounds by the Monte Carlo was checked by creating subsamples from the electron candidates enriched in the background. We calculate a correction factor, $C_{bkgd} = (N_{data} - N_{MC-other})/N_{MC-bkgd}$ where N_{data}, $N_{MC-bkgd}$ and $N_{MC-other}$ are the integrated numbers of events from the data sample, the Monte Carlo background and the other Monte Carlo events, respectively. The numbers of events are obtained from a reference distribution with the integration region chosen so that the statistical error on C_{bkgd} is minimized. The statistical error on C_{bkgd} is added to the uncertainty of the background estimate.

The largest source of background in the $\tau^- \to e^- \bar{\nu}_e \nu_\tau$ sample is from $\tau^- \to h^- \geq 1\pi^0 \nu_\tau$ decays, where h^- is either a π^- or K^-. Approximately one-half of the background in the electron sample has a cluster that is not associated to the track (see fig. 1(e)). Consequently we can check the modelling of the background by examining the jet mass distribution of those events. The

jet mass is calculated using the track information for one four-vector and the cluster direction and energy for the second four-vector (we assume that both particles are pions). A $\mathrm{d}E/\mathrm{d}x$ requirement is also added which reduces the electrons but not the hadrons from this sample. The $\tau^- \to \mathrm{h}^- \geq 1\pi^0\nu_\tau$ background gives a peak in the jet mass distribution close to the mass of the $\rho(770)$ while the contribution from other electron candidates gives a broad distribution (see fig. 2(a)). Comparisons of data and Monte Carlo suggest that the Monte Carlo overestimates the background and we apply a correction of 0.83 ± 0.06 to this background estimate.

The $\tau^- \to \mathrm{h}^-\nu_\tau$ background was checked by comparing the $N^\sigma_{E/p}$ distribution for data and Monte Carlo (see fig. 2(b)). We used our electron selection but with the $\mathrm{d}E/\mathrm{d}x$ requirement reversed so that hadrons instead of electrons were selected. The unshaded histogram shows the $\tau^- \to \mathrm{h}^-\nu_\tau$ background and the shaded histogram shows the other hadronic decays of the tau. The $N^\sigma_{E/p}$ distribution for hadrons from $\tau^- \to \mathrm{h}^-\nu_\tau$ decays can be roughly divided into two samples. Those with $N^\sigma_{E/p} \leq -5$ are more typical hadrons as they leave a small fraction of their energy in the electromagnetic calorimeter with the remaining energy being deposited in the hadron calorimeter. Hadrons with $N^\sigma_{E/p} \geq -5$ are less common but are strongly enhanced by our electron selection. These hadrons deposit most of their energy in the electromagnetic calorimeter. As a result we use the region $-4 \leq N^\sigma_{E/p} \leq 0$, which corresponds to the region included in our selection, to obtain a correction factor of 1.25 ± 0.14. The modelling of the $N^\sigma_{E/p}$ distribution in fig. 2(b) is not ideal. If we change the $N^\sigma_{E/p}$ criterion in the Electron Identification selection and recalculate the correction factors for the new region, however, we obtain a branching ratio consistent with our result.

The $\mathrm{e}^+\mathrm{e}^- \to \mathrm{e}^+\mathrm{e}^-$ events that pass the electron selection tend to be events with final state radiation. The tau pair selection removes the non-radiative $\mathrm{e}^+\mathrm{e}^- \to \mathrm{e}^+\mathrm{e}^-$ events with cuts on the total electromagnetic energy in the event while the electron selection eliminates events where there are back-to-back tracks with the acoplanarity requirement. We found that the $\mathrm{e}^+\mathrm{e}^- \to \mathrm{e}^+\mathrm{e}^-$ events with little radiation were well described by the Monte Carlo. In fig. 2(c) we plot $E_{\mathrm{cluster}}/E_{\mathrm{CM}}$ for jets that pass the electron selection. The unshaded histogram is the tau Monte Carlo and the shaded histogram is the $\mathrm{e}^+\mathrm{e}^- \to \mathrm{e}^+\mathrm{e}^-$ Monte Carlo. The $\mathrm{e}^+\mathrm{e}^- \to \mathrm{e}^+\mathrm{e}^-$ Monte Carlo overestimates the background and we apply a correction factor of 0.55 ± 0.09 to the background estimate obtained from the Monte Carlo.

The final background is due to events from the $\mathrm{e}^+\mathrm{e}^- \to (\mathrm{e}^+\mathrm{e}^-)\,\mathrm{e}^+\mathrm{e}^-$ reaction. The incoming electron and positron exit the detector undetected leaving a relatively low momentum electron-positron pair. To enhance these events, we create a sample where both jets pass our electron selection. In fig. 2(d) we plot the ratio $E_{\mathrm{visible}}/E_{\mathrm{CM}}$. The unshaded histogram is the tau Monte Carlo and the shaded histogram is the $\mathrm{e}^+\mathrm{e}^- \to (\mathrm{e}^+\mathrm{e}^-)\,\mathrm{e}^+\mathrm{e}^-$ Monte Carlo. We find that the Monte Carlo overestimates the background and we apply a correction factor of 0.7 ± 0.2.

The $\tau^- \to \mathrm{e}^-\bar{\nu}_\mathrm{e}\nu_\tau$ branching ratio was previously measured by OPAL to be $(18.04 \pm 0.33)\%$ [8] using data collected between 1990 and 1992. The current result, $(17.78 \pm 0.10 \pm 0.09)\%$, is consistent with the previous work, using a quite different selection procedure and with approximately three times the data sample. In addition, the branching ratio is consistent with other results, including recent measurements by ALEPH [13] of $(17.79 \pm 0.12 \pm 0.06)\%$ and DELPHI [14] of $(17.51 \pm 0.39)\%$. The 1994 Particle Data Group average value is $(17.90 \pm 0.17)\%$[15].

The $\tau^- \to \mathrm{e}^-\bar{\nu}_\mathrm{e}\nu_\tau$ branching ratio can be used to test lepton universality. The ratio of the

widths for $\tau^- \to \mu^- \bar{\nu}_\mu \nu_\tau$ and $\tau^- \to \mathrm{e}^- \bar{\nu}_\mathrm{e} \nu_\tau$ gives a measure of g_μ/g_e [16]

$$\frac{\Gamma(\tau^- \to \mu^- \bar{\nu}_\mu \nu_\tau)}{\Gamma(\tau^- \to \mathrm{e}^- \bar{\nu}_\mathrm{e} \nu_\tau)} = \frac{g_\mu^2}{g_e^2} \frac{f(m_\mu^2/M_\tau^2)}{f(m_e^2/M_\tau^2)}$$

where g_μ and g_e are the electroweak coupling constants for the muon and electron, and $f(x) = 1-8x+8x^3-x^4-12x^2\ln x$. Using the latest measurement of the τ mass by the BES Collaboration of $1776.96^{+0.18+0.25}_{-0.21-0.17}\,\mathrm{MeV/c^2}$ [17] and the OPAL $\tau^- \to \mu^- \bar{\nu}_\mu \nu_\tau$ branching ratio of $(17.36 \pm 0.27)\%$ [8], we obtain $g_\mu/g_e = 1.0016 \pm 0.0087$. Note, however, that the most precise test of this universality (at the level of 0.002) has been made by measuring the pion leptonic branching ratios [18].

A test of muon-tau universality can be made by comparing the partial widths for the $\tau^- \to \mathrm{e}^- \bar{\nu}_\mathrm{e} \nu_\tau$ and $\mu^- \to \mathrm{e}^- \bar{\nu}_\mathrm{e} \nu_\mu$ decays, which have the form [16]

$$\frac{g_\tau^2}{g_\mu^2} = 0.9996 \frac{\tau_\mu}{\tau_\tau} \frac{m_\mu^5}{m_\tau^5} B(\tau^- \to \mathrm{e}^- \bar{\nu}_\mathrm{e} \nu_\tau)$$

Using the OPAL tau lifetime measurement of $288.8 \pm 2.2 \pm 1.4$ fs [19], we obtain $g_\tau/g_\mu = 1.0025 \pm 0.0060$. The OPAL tau lifetime and $\tau^- \to \mathrm{e}^- \bar{\nu}_\mathrm{e} \nu_\tau$ branching ratio are plotted in fig. 3. The band is the Standard Model prediction assuming lepton universality. The width of the band corresponds to the uncertainty in the tau mass.

The strong coupling α_s can be extracted from $R_\tau = B(\tau^- \to \mathrm{hadrons}^- \nu_\tau)/B(\tau^- \to \mathrm{e}^- \bar{\nu}_\mathrm{e} \nu_\tau)$ using the leptonic branching ratios and the τ lifetime. In an earlier OPAL publication, $R_\tau = 3.654 \pm 0.038$ was determined using the leptonic branching ratio based on 1990-1992 data [8] and the lifetime based on 1990-1993 data [19]. We follow the same prescription that was described in detail in ref. [8]. Our new measurement of $B(\tau^- \to \mathrm{e}^- \bar{\nu}_\mathrm{e} \nu_\tau)$, together with the τ lifetime and $\tau^- \to \mu^- \bar{\nu}_\mu \nu_\tau$ branching ratio, gives $R_\tau = 3.659 \pm 0.030$. The resulting α_s value is $0.377^{+0.015+0.026}_{-0.014-0.018}$ at $Q^2 = M_\tau^2$ and $0.1231 \pm 0.0013^{+0.0025}_{-0.0021}$ at $Q^2 = M_Z^2$ where the first error is experimental and the second error is theoretical. Note, however, there may be an additional uncertainty of as much as ± 0.002 [20] or ± 0.005 [21] from effects beyond the SVZ parameterization [22] used to determine the coupling constant.

In summary, the branching ratio of the $\tau^- \to \mathrm{e}^- \bar{\nu}_\mathrm{e} \nu_\tau$ decay was measured using the 1991-1994 data samples recorded using the OPAL detector to be

$$B(\tau^- \to \mathrm{e}^- \bar{\nu}_\mathrm{e} \nu_\tau) = (17.78 \pm 0.10 \pm 0.09)\%$$

This new branching ratio supersedes the previous OPAL measurement and is consistent with the results of other experiments. The branching ratio has been used together with other measurements to test $e-\mu$ and $\mu-\tau$ lepton universality. The results indicate that the hypotheses of lepton universality in the charged current weak interaction are valid to within the 1% level.

Acknowledgements:

It is a pleasure to thank the SL Division for the efficient operation of the LEP accelerator, the precise information on the absolute energy, and their continuing close cooperation with our experimental group. In addition to the support staff at our own institutions we are pleased to acknowledge the
Department of Energy, USA,
National Science Foundation, USA,
Particle Physics and Astronomy Research Council, UK,
Natural Sciences and Engineering Research Council, Canada,
Fussefeld Foundation,
Israel Ministry of Science,
Israel Science Foundation, administered by the Israel Academy of Science and Humanities,
Minerva Gesellschaft,
Japanese Ministry of Education, Science and Culture (the Monbusho) and a grant under the Monbusho International Science Research Program,
German Israeli Bi-national Science Foundation (GIF),
Direction des Sciences de la Matière du Commissariat à l'Energie Atomique, France,
Bundesministerium für Forschung und Technologie, Germany,
National Research Council of Canada,
A.P. Sloan Foundation and Junta Nacional de Investigação Científica e Tecnológica, Portugal.
Hungarian Foundation for Scientific Research, OTKA T-016660.

References

[1] OPAL Collaboration, K. Ahmet *et al.*, Nucl. Instr. and Meth. **A305** (1991) 275.

[2] S. Jadach, B. F. L. Ward, and Z. Was, Comp. Phys. Comm. **79** (1994) 503; (KORALZ Version 4.0).

[3] S. Jadach, J. H. Kühn, and Z. Was, Comp. Phys. Comm. **76** (1993) 361; (TAUOLA Version 2.0).

[4] R. Brun et al., GEANT 3, Report DD/EE/84-1, CERN (1989).

[5] J. Allison et al., Comp. Phys. Comm. **47** (1987) 55.

[6] OPAL Collaboration, G. Alexander *et al.*, Phys. Lett. **B266** (1991) 201.

[7] OPAL Collaboration, P. Acton *et al.*, Phys. Lett. **B288** (1992) 373.

[8] OPAL Collaboration, R. Akers *et al.*, Z. Phys. **C66** (1995) 543.

[9] OPAL Collaboration, G. Alexander *et al.*, Z. Phys. **C52** (1991) 175.

[10] M. Böhm, A. Denner and W. Hollik, Nucl. Phys. **B304** (1988) 687;
F. A. Berends, R. Kleiss, W. Hollik, Nucl. Phys. **B304** (1988) 712; (BABAMC).

[11] T. Sjöstrand, Comp. Phys. Comm. **39** (1986) 347;
T. Sjöstrand, Comp. Phys. Comm. **43** (1987) 367;
T. Sjöstrand, CERN-TH-6488/92.; (JETSET, Version 7.3).

[12] R. Bhattacharya, J. Smith, G. Grammer, Phys. Rev. **D15** (1977) 3267;
J. Smith, J. A. M. Vermaseren, G. Grammer, Phys. Rev. **D15** (1977) 3280;
(Vermaseren, Version 1.01).

[13] ALEPH Collaboration, D. Buskulic *et al.*, CERN Preprint CERN-PPE/95-127.

[14] DELPHI Collaboration, P. Abreu *et al.*, CERN Preprint CERN-PPE/95-114.

[15] Review of Particle Properties, L. Montanet *et al.*, Phys. Rev. **D50** (1994) 1173.

[16] W.J. Marciano and A. Sirlin, Phys. Rev. Lett. **61** (1988) 1815.

[17] BES Collaboration, J.Z. Bai *et al.*, SLAC Preprint SLAC-PUB-6930.

[18] D. Britton *et al.*, Phys. Rev. Lett. **68** (1992) 3000.
G. Czapek *et al.*, Phys. Rev. Lett. **70** (1993) 17.

[19] OPAL Collaboration, R. Akers *et al.*, Phys. Lett. **B338** (1994) 497.

[20] S. Narison, Proceedings of the Third Workshop on Tau Lepton Physics, Montreux, (1994), CERN-TH 7506 (1994)

[21] G. Altarelli, P. Nason and G. Ridolphi, CERN-TH 7537 (1994)

[22] M. A. Shifman, A. L. Vainstein and V. I. Zakharov, Nucl. Phys. **B147** (1979) 385,448,519.

Table 1: Estimated backgrounds after applying corrections

Background	Corrected Contamination
	τ pairs
$e^+e^- \to \mu^+\mu^-$	0.0072 ± 0.0005
$e^+e^- \to q\overline{q}$	0.0042 ± 0.0008
$e^+e^- \to e^+e^-$	0.0041 ± 0.0007
$e^+e^- \to (e^+e^-)\,\mu^+\mu^-$	0.0008 ± 0.0002
$e^+e^- \to (e^+e^-)\,e^+e^-$	0.0007 ± 0.0002
Total	0.0170 ± 0.0012
	$\tau^- \to e^-\bar{\nu}_e\nu_\tau$
$\tau^- \to h^- \geq 1\pi^0\nu_\tau$	0.0253 ± 0.0020
$\tau^- \to h^-\nu_\tau$	0.0139 ± 0.0017
$e^+e^- \to e^+e^-$	0.0057 ± 0.0013
$e^+e^- \to (e^+e^-)\,e^+e^-$	0.0038 ± 0.0011
other τ decays	0.0009 ± 0.0004
Total	0.0496 ± 0.0031

Table 2: Efficiencies of Fiducial Selection

Description	Efficiency
z-chamber acceptance	0.93905 ± 0.00066
EM calorimeter acceptance	0.9835 ± 0.0004
z-chamber hits (1 tk)[1]	$0.91619 \pm 0.00079 \pm 0.00160$
z-chamber hits (2,3 tk)	0.85 ± 0.05
dE/dx hits (1 tk)[1]	$0.99210 \pm 0.00024 \pm 0.00050$
dE/dx hits (2 tk)	1.00 ± 0.05
dE/dx hits (3 tk)	0.90 ± 0.05

[1] Here we give the average efficiency whereas in the actual selection the momentum dependent efficiency is used.

Table 3: Systematic Errors

electron background	0.00058
electron identification selection efficiency	0.00048
bias factor	0.00039
fiducial selection efficiency	0.00028
non-tau background	0.00022
photon conversions	0.00006
Total	0.00093

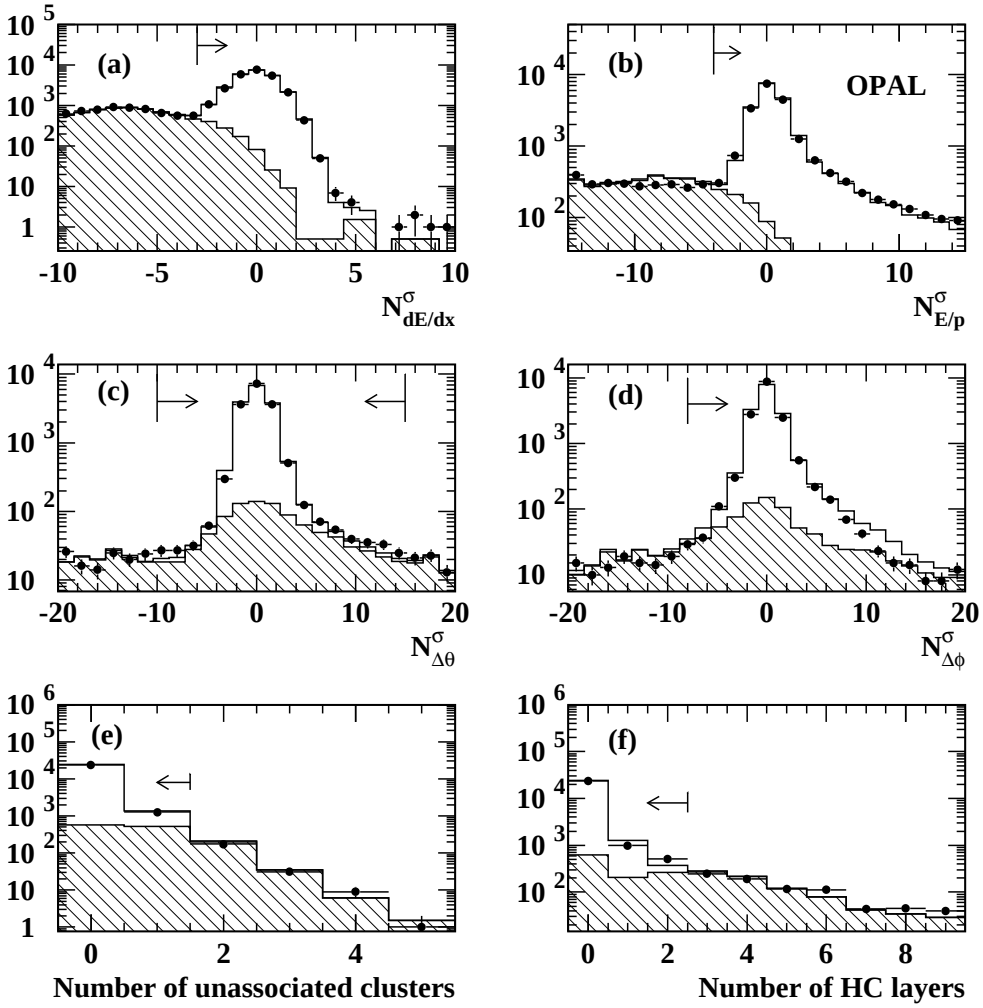

Figure 1: The main variables used in the electron selection are plotted: (a) the normalized $\mathrm{d}E/\mathrm{d}x$, (b) the normalized E/p, (c) the normalized $\Delta\theta$, (d) the normalized $\Delta\phi$, (e) the number of clusters not associated to a charged track and (f) the number of hadron calorimeter layers. The data are represented by points and the Monte Carlo prediction is represented by the unshaded histogram. The shaded region of the histogram is the Monte Carlo prediction for the background. The data shown in each plot are required to pass the electron selection except for the variable displayed. The arrows indicate the regions accepted in the selection.

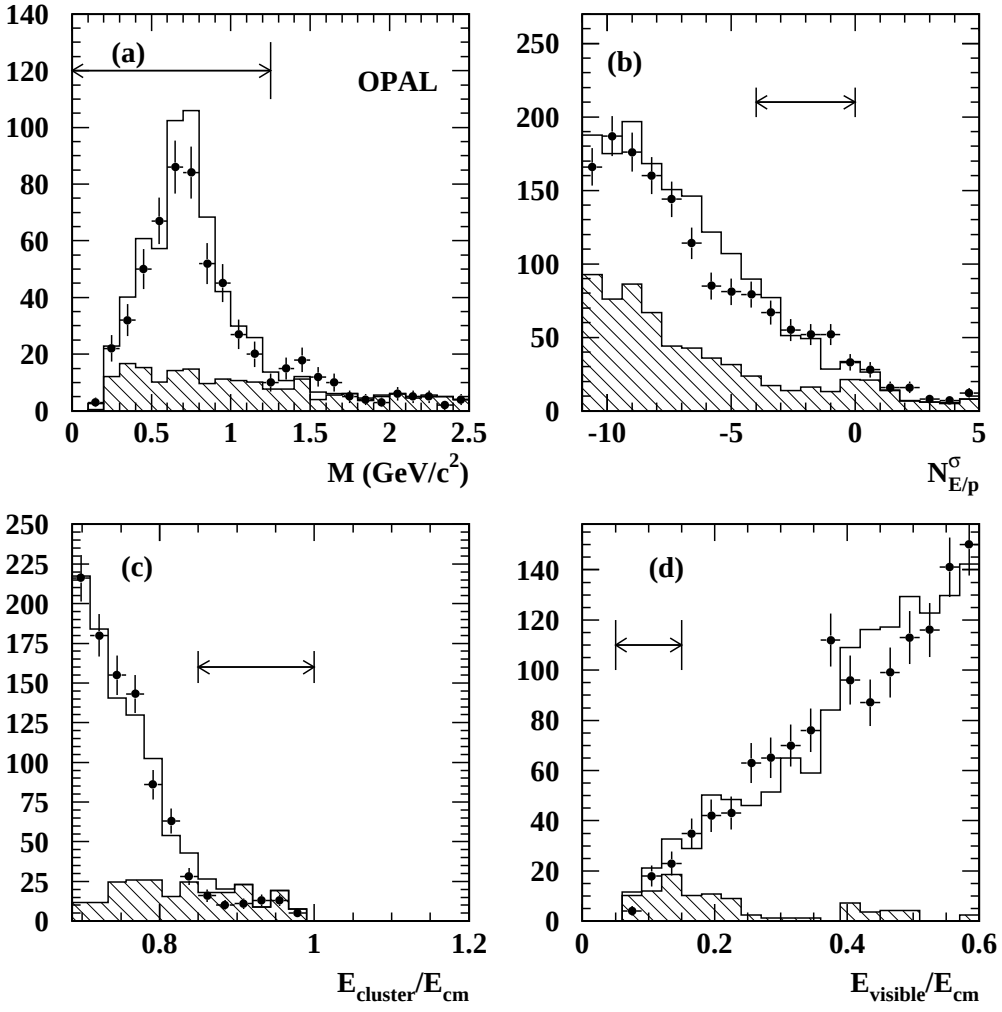

Figure 2: The distributions used to obtain the background correction factors are shown. The data are represented by the points and the Monte Carlo prediction is represented by the histogram. Figure (a) is the mass distribution used to estimate the $\tau^- \to h^- \geq 1\pi^0\nu_\tau$ background correction. The unshaded portion of the histogram shows the $\tau^- \to h^- \geq 1\pi^0\nu_\tau$ decays and shaded portion shows the other tau decays. Figure (b) is the $N^{\sigma}_{E/p}$ distribution used to estimate the $\tau^- \to h^-\nu_\tau$ background correction. The unshaded portion shows the $\tau^- \to h^-\nu_\tau$ decays and shaded portion shows the other tau decays. Figure (c) is the $E_{\rm cluster}/E_{\rm CM}$ distribution used to estimate the $e^+e^- \to e^+e^-$ background correction. The unshaded portion shows the tau decays and the shaded portion shows the $e^+e^- \to e^+e^-$ events that pass the electron selection. Figure (d) is the $E_{\rm visible}/E_{\rm CM}$ distribution used to estimate the $e^+e^- \to (e^+e^-)\,e^+e^-$ background correction. The unshaded portion shows the tau decays and the shaded portion shows the $e^+e^- \to (e^+e^-)\,e^+e^-$ events where both jets pass the electron selection. The arrows indicate the regions used to determine the correction factors.

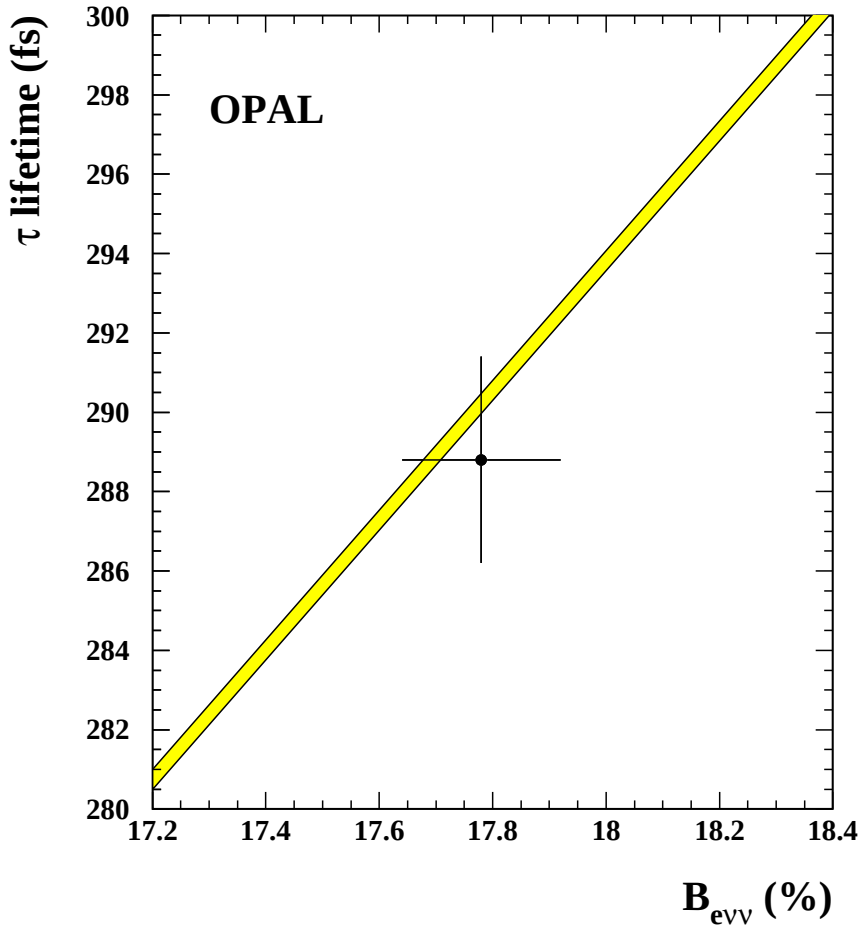

Figure 3: The electronic branching ratio of the tau is plotted against the OPAL tau lifetime. The band is the prediction assuming $\mu - \tau$ universality and its width reflects the uncertainty associated with the tau mass.